Remote Sensing of Environment 183 (2016) 318–333

Contents lists available at ScienceDirect

Remote Sensing of Environment

journal homepage: www.elsevier.com/locate/rse

Lidar detection of individual tree size in tropical forests

António Ferraz [a,*], Sassan Saatchi [b], Clément Mallet [c], Victoria Meyer [b,d]

[a] NASA Postdoctoral Program fellow, Jet Propulsion Laboratory, California Institute of Technology, 4800 Oak Grove Drive, Pasadena, CA 91109, USA
[b] Jet Propulsion Laboratory, California Institute of Technology, 4800 Oak Grove Drive, Pasadena, CA 91109, USA
[c] Institut National de l'Information Géographique et Forestière (IGN), LaSTIG, MATIS, Université Paris-Est, 94160 Saint Mandé, France
[d] Laboratoire Evolution et Diversité Biologique UMR CNRS 5174, CNRS Université Paul Sabatier, Toulouse, France

ARTICLE INFO

Article history:
Received 20 November 2015
Received in revised form 24 May 2016
Accepted 31 May 2016
Available online xxxx

Keywords:
Airborne lidar
3D tropical forest structure modeling
Mean shift algorithm segmentation
Individual tree detection
Tropical tree crown clustering
Crown area
Crown volume
Carbon estimation
Aboveground biomass

ABSTRACT

Characterization of tropical forest trees has been limited to field-based techniques focused on measurement of diameter of the cylindrical part of the bole, with large uncertainty in measuring large trees with irregular shapes, and other size attributes such as total tree height and the crown size. Here, we introduce a methodology to decompose lidar point cloud data into 3D clusters corresponding to individual tree crowns (ITC) that enables the estimation of many biophysical variables of tropical forests such as tree height, crown area, crown volume, and tree number density. The ITC-based approach was tested using airborne high-resolution lidar data collected over the 50-ha Center for Tropical Forest Science (CTFS) plot in the Barro Colorado Island, Panama. The lack of tree height and crown size measurements in the field prohibits the direct validation of the ITC metrics. We assess the reliability of our method by comparing the aboveground biomass (AGB) estimated using ground and lidar individual tree measurements at multiple spatial scales, namely 1 ha, 2.25 ha, 4 ha, and 6.25 ha. We examined four different lidar-derived AGB models, with three based on individual tree height, crown volume, and crown area, and one with mean top canopy height (TCH) calculated at the plot level using the lidar canopy height model. Results show that the predictive power of all models based on ITC size and TCH increases with decreasing spatial resolution from 16.9% at 1 ha for the worst model to 5.0% at 6.25 ha for the best model. The TCH-based model performed slightly better than ITC-based models except at higher spatial scales (~4 ha) and when errors due to edge effects associated with tree crowns were reduced. Unlike the TCH models that change regionally depending on forest type and structure allometry, the ITC-based models are derived as a function of individual tree allometry and can be extended globally to all tropical forests. The method for lidar detection of individual crown size overcome some limitations of ground-based inventories such as 1) it is able to access crowns of large trees and 2) it enables the assessment of directional changes in tree density, canopy architecture and forest dynamics over large and inaccessible areas to support robust tropical ecological studies.

1. Introduction

Canopy environments, where tree stems, branches and leaves reside, mediate the entire ecosystem exchange of water and carbon with the atmosphere by influencing transpiration and the photosynthetic production (Malhi, Doughty, & Galbraith, 2011). Other ecosystem functions such as biological diversity, growth, mortality and recruitment also depend significantly on the structure of the canopy and light conditions (Stark et al., 2012). However, the exact nature and function of tree canopies are not well known, particularly in tropical environments where diversity of species, complexity of tree structure, crown shape and size makes direct measurements difficult. In fact, the characterization of the three-dimensional (3D) canopy structure across different geographical zones to model variables that control tropical forest dynamics and biomass variations is lacking. In practice, field-sampling techniques are often limited to small areas, and mainly focused on horizontal components of structure such as tree density, basal area, and species abundance. This is mainly due to dense and complex vertical structure of tropical forests, preventing surveyors from easily targeting the tree height and crown edges from the ground. As a result, the tree height (TH), a variable that along with the diameter at breast height (DBH) significantly determines the amount of biomass of trees (Chave et al., 2005), has been estimated by applying allometric models to DBH measurements, (Chave et al., 2014; Feldpausch et al., 2011). Although there are relevant allometric relationships between DBH and TH on the average regionally, they are not suited to capture the variability across forest types landscapes, and may introduce large uncertainty in estimating forest structure and biomass locally (Ngomanda et al., 2014; Saatchi et al., 2015). Furthermore, most large tropical trees that contain a significant portion of the forest biomass develop irregularly shaped buttresses, making the diameter measurements in the field difficult and with large uncertainty. In addition to DBH and TH, the crown size also impacts the tree biomass by holding more than 30% of total

* Corresponding author.
E-mail address: Antonio.A.Ferraz@jpl.nasa.gov (A. Ferraz).

http://dx.doi.org/10.1016/j.rse.2016.05.028
0034-4257/

biomass in coarse and fine branches, leaves, and fruits (Goodman, Phillips, & Baker, 2014; Ploton et al., 2015). However, there is almost no widely used allometric model that relates tree size (either DBH or TH) to crown area (CA) or crown volume (CV) for tropical forests except in local studies (Bohlman & O'Brien, 2006).

Remote sensing (RS) techniques with capability of quantifying forest structure in both vertical and horizontal dimensions and extensively over the landscapes, such as lidar (Light Detection and Ranging) or radar (Radio Detection and Ranging), are considered alternative or complementary methods to circumvent the difficulty of field techniques (Ferraz et al., 2015; Hall et al., 2011; Wulder et al., 2012). Most existing RS techniques rely on developing allometric models between height metrics and field-estimated forest biomass (Asner et al., 2013; Meyer et al., 2013). However, methods to provide direct estimation of tree level forest structure that can potentially eliminate ground measurements of structure in tropical forests are yet to be developed (Hyyppä et al., 2008; Zolkos, Goetz, & Dubayah, 2013). There have been some efforts in temperate and boreal forests to use high-resolution multi- or hyper-spectral imagery and directly extract individual tree crown (ITC) size, which is subsequently used in biomass estimation (Hyyppä et al., 2008; Ke & Quackenbush, 2011). However, the ITC extraction methodology with imagery has not been very successful in tropical forests due to complex and challenging forest structure, overlapping crowns and multiple species (Asner et al., 2002; Féret & Asner, 2013). Indeed, the extraction rate of such approaches is still low and relies on many parameters that need to be locally calibrated. In addition, they are limited to the topmost trees (Tochon et al., 2015). There is a strong indication that high-resolution lidar measurements are able to characterize both the top canopy and understory trees but an approach able to extract ITC is lacking (Detto, Asner, Muller-landau, & Sonnentag, 2015; Hunter et al., 2015).

Here, we present a two-step approach that extracts ITC using lidar data over tropical forests. In the first step, we extract easily recognizable individual trees (e.g. isolated) from the lidar data in order to derive local tree allometry relating tree height to crown size. In the second step, tree allometry is used to calibrate an existing technique called 3D Adaptive Mean Shift (AMS3D) that decomposes the entire point cloud into 3D clusters that correspond to ITC (Ferraz et al., 2012). The AMS3D technique allows to retrieve many forest metrics (e.g. tree density, tree height and crown volume) that can be readily included in an allometric model to estimate the aboveground biomass. We apply the methodology to lidar data collected over a 50 ha forest inventory plot located in a rain forest research site in the Barro Colorado Island (BCI, Panama). Results are compared with field-derived biomass and the application of the methodology for a global use and sources of uncertainty of the methodology are identified and discussed.

2. Materials

2.1. Study area and inventory data

The study area is a 50 ha (1000 m × 500 m) old-growth forest plot managed by the Center for Tropical Forest Science (CTFS, Condit, Engelbrecht, Pino, Pérez, & Turner, 2013; Condit, 1998; Hubbell et al., 1999) located in Barro Colorado Island (BCI) in the Panama Canal (Fig. 1). This low elevation area is located in the center of the island and the inventory data have been collected every five years since 1982 (Hubbell & Foster, 1983). In this work, we use the 2010 census data that includes all trees with a diameter at breast height (DBH) greater than 1 cm, with measurements made higher on the bole for individuals with buttresses or trunk irregularities. The location of each tree and the species are identified, allowing us to examine potential correspondence with the high-resolution lidar observation.

We included additional measurements on both tree height (TH) and crown width (CW) for 1604 individuals collected within the 50 ha plot during the dry season of 1993 and 1997 for allometric model development purposes (Bohlman & O'Brien, 2006). The measurements do not include all trees in a systematic way and only focused in 83 dominant species.

2.2. Airborne lidar scanning data

The airborne lidar scanning data were acquired during the wet season of the year of 2009 in 11 separate flights between August 15 and September 10 using an Optech ALTM 3100 scanning device (Table 1) and were collected by the Blom Corporation and Northrop Grumman, as part of an NSF project (Lobo & Dalling, 2014; Meyer et al., 2013). The lidar data were processed to provide geo-referenced 3D point clouds. The position and orientation of platform, which are given by onboard GPS/IMU measurements, were corrected by analyzing overlapping laser strips from the calibration flight lines (TerraMatch, Burman & Soininen, 2004). These parameters, together with the GPS measurements acquired during the flight using a reference ground station, provided a point cloud in the WGS84/UTM zone 17N coordinate system for further processing. After removing of non-valid points the remaining points were assigned to a single class: ground or off-ground points (TerraScan, Soininen, 2011).

The average point density over the 50 ha plot is 10.8 pt/m^2. To calculate the effective height of trees the effect of topography on the lidar measurements was removed by normalizing the point cloud using the lidar derived Digital Terrain Model (DTM, 0.3 m × 0.3 m) that have been interpolated from a Delaunay triangulation defined as a function of the lidar points corresponding to the ground. The area is characterized by a low topographic variation and the DTM accuracy is not expected to impact on the results. All lidar points lower than 2 m height were removed from the point cloud for reducing the processing time. Furthermore, this does not impact the results because we focus on trees with DBH larger than 10 cm corresponding to trees higher than 10 m and with a crown base height of nearly 7 m according to local field measurements (Bohlman & O'Brien, 2006).

3. Method

Here we develop a new method (Section 3.2) designed to provide the a priori information required by an existing algorithm called 3D Adaptive Mean Shift (AMS3D, Section 3.1 and Fig. 2) to properly extract individual trees over tropical forests structures. The AMS3D decomposes lidar point clouds into 3D clusters that correspond to individual tree crowns (ITC) providing a fully characterization of the entire forest scene. It is able to deal with trees located within every forest layer from the overstory to the understory. The method is only briefly described in Section 3.1 but details of its mathematical formulation can be found in Ferraz et al. (2012). It depends on a single parameter called bandwidth that corresponds to the volume of a 3D kernel (blue cylinder in *Bandwidth model* module, Fig. 2) that is used for the statistical analysis in the neighborhood of each 3D lidar point. In order to capture the complexity of trees, the AMS3D requires an adaptive bandwidth such that the diameter and height of the 3D kernel would approximate the mean diameter and depth of crowns for a given forest height, respectively. That is, the knowledge of a proxy for the local tree allometry is crucial to properly extract individual trees using the AMS3D. In Ferraz et al. (2012), the authors defined three bandwidths of different sizes to apply to three forest layers: overstory, understory and ground vegetation. However, this approach is not suitable for tropical forest because the boundaries of the layers are fuzzy and difficult to identify (Jaskierniak, Lane, Robinson, & Lucieer, 2011).

In this work, we developed a methodology to estimate tree size allometry directly from the lidar data in order to locally calibrate the bandwidth model (Section 3.2 and Fig. 2). In fact, the bandwidth model could be ideally calibrated using tree allometry derived from ground measured height, crown diameter and crown depth. However, because of the paucity of inventory data over tropical regions, the

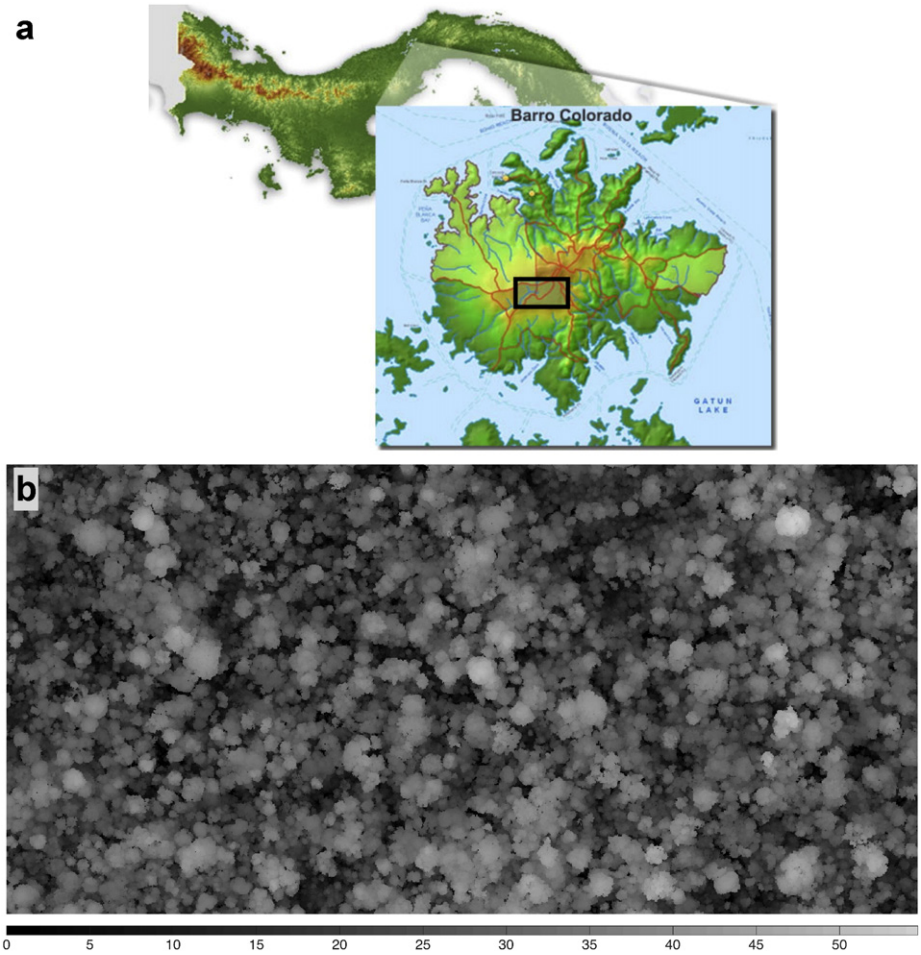

Fig. 1. Experiment **a)** location in Barro Colorado Island (Panama) with the 50 ha (100 m × 50 m) plot represented by a black rectangle and **b)** corresponding canopy height model (1 m × 1 m) calculated using the lidar data (Section 2.2). Color bar represents height in meters. (For interpretation of the references to color in this figure legend, the reader is referred to the web version of this article.)

calibration of the bandwidth would be limited and extensively applicable. Therefore, we established a self-calibrated bandwidth model that can adapt to the local forest structure. First, we developed an object-oriented approach to delineate a limited number of easily distinguishable individual crown boundaries using a canopy height model (CHM, Section 3.2.1 in Fig. 2). Although these few samples could help to estimate the tree height to crown width allometric equation, they are of little use in developing the tree height to crown depth relationship. As a result, we overlay the individual crown boundaries delineated on the CHM to the lidar point cloud in order to extract the 3D ITC samples (Section 3.2.2 in Fig. 2). The latter allow us to derive the relationship between tree height and both crown width and depth (Section 3.2.3 in Fig. 2). This tree allometry defines the bandwidth model, which corresponds to a continuous monotonically increasing function that forces the 3D kernel volume to increase as it moves to higher lidar points. Then, the bandwidth model is used to tune the AMS3D algorithm that applies directly to the lidar point cloud to calculate the 3D clusters that correspond to individual trees (colored lidar points in Section 3.1, Fig. 2). Many biophysical metrics can be derived from such ITC maps. In this work, we calculate tree number density, tree location (barycenter of the x and y coordinates of the 3D cluster) and, tree height (z coordinate of the highest lidar point for 3D each cluster). Moreover, we model the 3D clusters using a convex hull to calculate both the crown area (CA) and the crown volume (CV) for individual trees (Silva, Crookston, Hudak, & Vierling, 2015). The methodology used to validate the reliability of our method to characterize the forest structure variability is explained in Section 3.3.

Table 1
Lidar acquisition parameters.

Lidar sensor	Optech ALTM 3100
Wavelength	1064 nm
Scan angle	34°
Pulse rate	70 kHz
Effective measurement rate	48 kHz
Ground speed	66.9 m/s
Flying height	457.2 m
Swath width	279.2 m
Swath overlap	45.7%
Average point density	10.8 pt/m^2

3.1. Adaptive mean shift 3D segmentation (AMS3D)

The AMS3D decomposes a lidar point cloud into 3D clusters corresponding to ITC. It is a two-step approach that assumes the point cloud to be a multi-modal distribution where each mode, defined as a local maximum in both density and height, corresponds to a single location within an individual crown. The first step consists in calculating the multiple modes of the point cloud using a 3D kernel that is iteratively moved to denser regions until convergence. In practice, a 3D kernel is defined over each lidar point in order to compute the local barycenter of the lidar point cloud, which is then shifted from the original location to the local barycenter. This procedure leads the 3D kernel to converge

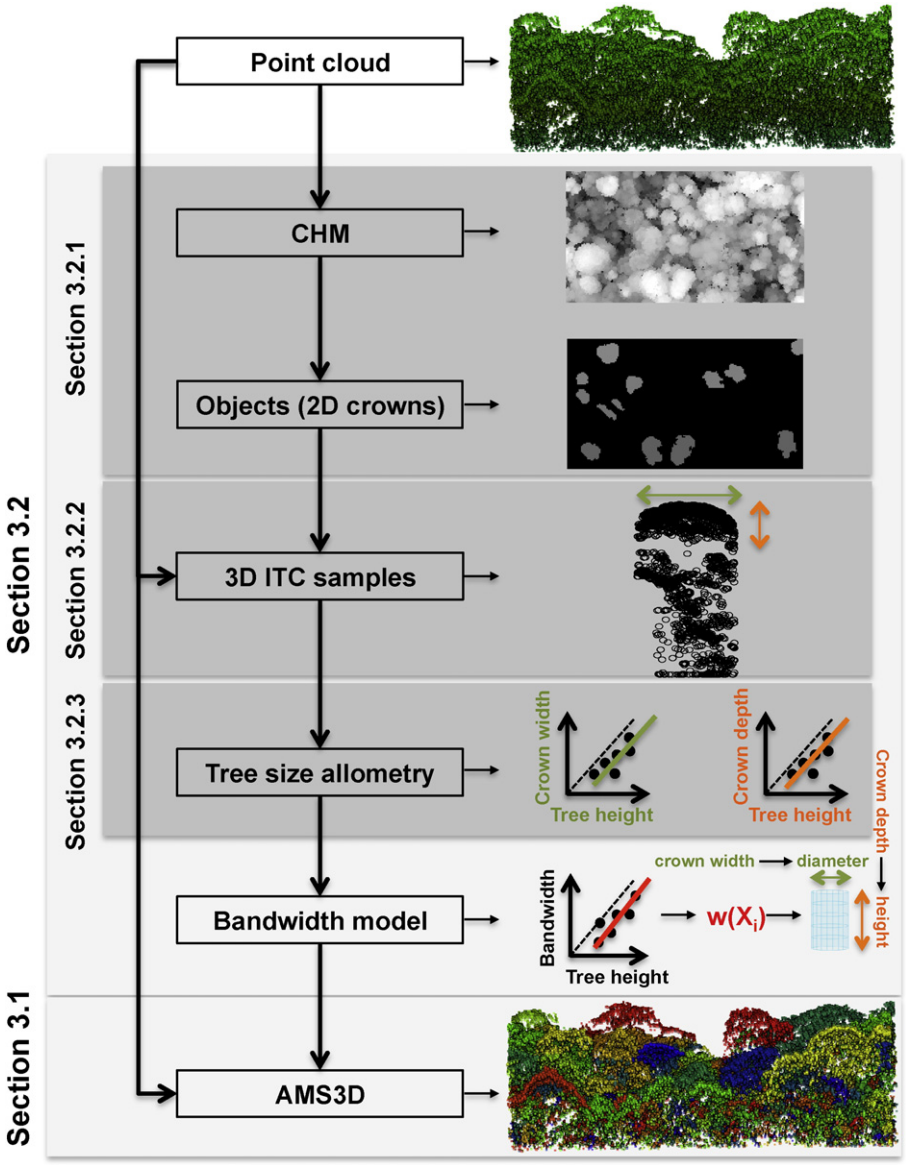

Fig. 2. Methodology workflow showing $w(X_i)$ referring to the bandwidth model function shown in Fig. 3 and the blue cylinder representing the 3D kernel. CHM and ITC stand for canopy height model and individual tree crown, respectively. (For interpretation of the references to color in this figure legend, the reader is referred to the web version of this article.)

to the local mode. In the second step, the 3D clusters corresponding to ITC are computed by gathering together the lidar points that are converged to the same mode (Fig. 3).

The AMS3D has two main advantages that lead us to investigate its ability for the characterization of complex tropical forest structures. First, it can deal with crowns with different shapes (e.g. atypical, ellipsoidal, conical) because it is a non-parametric approach that does not make any assumption on the outline of the objects of interest. Second, it only depends on a single parameter, which is the size of the 3D kernel that we named bandwidth. The latter determines the magnitude of the decomposition of the lidar point cloud by defining the number of 3D clusters and therefore the tree density for a given area. A small bandwidth would seek for local maxima within a narrow neighborhood leading to a tree density overestimation because larger trees would be split into several smaller crowns. In contrast, a large bandwidth would look for local maxima in a broad neighborhood, clustering together many small trees leading to a tree density underestimation. As a result, a single bandwidth is not adapted to analyze forest stand that display heterogeneous crown sizes. In the following we present a bandwidth model defined as a continuous monotonically increasing function where the bandwidth increases as long as it applies to higher lidar points ($w(X_i)$ in Fig. 3).

3.2. Bandwidth model

Eq. (1) is a continuous function that represents the bandwidth model (w) that depends on the location and height of the lidar points (Ferraz et al., 2012):

$$w(X_i) = (w^s(X_i), w^z(X_i)) \quad (1)$$

where w^s and w^z are the horizontal and vertical components of the 3D kernel bandwidth (i.e. the diameter and height of the cylinders in Fig. 3), $X_i = (x_i, y_i, z_i)$ are the 3D coordinates of the lidar points and therefore X_i $(i = 1, \ldots, n)$ represents a point cloud that comprises n points. Our goal is to define both $w^s(X_i)$ and $w^z(X_i)$ in such a way that they approximate the mean crown width (CW) and the mean crown depth (CD) of individual trees for every forest height z_i, respectively. For such a purpose, we derive allometric equations (TH-CW and TH-CD, where TH stands for tree height) directly from the lidar data (Fig. 2).

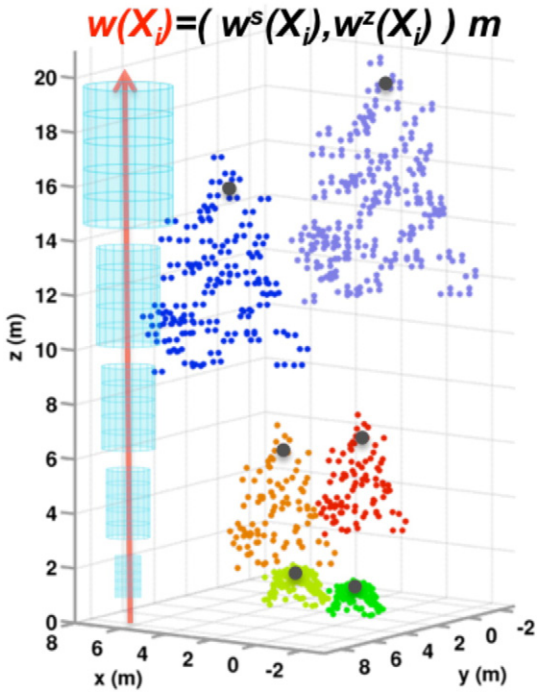

Fig. 3. AMS3D segmentation of a simulated forest scene using a cylindrical kernel whose diameter (w^s) and height (w^z) are defined by the bandwidth model w (X_i), with $X_i = (x_i,y_i,z_i)$, that depends on the lidar point's height z_i. Colored dots correspond to 3D clusters of lidar points gathered around the local modes (gray dots) to represent individual tree crowns. (For interpretation of the references to color in this figure legend, the reader is referred to the web version of this article.)

3.2.1. CHM-based 2D individual crowns samples extraction

The purpose of the CHM-based approach is not to attain a high percentage of detected trees. Instead, we intend to accurately estimate the size of some ITC samples by focusing on the delineation of crowns that are easily distinguishable in the CHM data. This approach is based on three standard assumptions: 1) CHM is significantly lower in the surroundings of the crown envelop (ITC outside perimeter) than within it, 2) the ITC outside perimeter is ellipse-shaped, and 3) the ratio of tree height to crown width is within a certain realistic range.

Our approach is an image processing method that consists of a) a pixel-based image analysis followed by b) an object-based image analysis (OBIA, Fig. 4):

a) First, we developed a filter called multi-directional gradient filter that looks for significant elevation change according to eight different directions in order to enhance the humps of the CHM that are likely to correspond to individual crowns (Fig. 4). We carry out a multi-scale analysis by applying the referred filter at several spatial resolutions that allow capturing crowns of different sizes. This procedure provides several images (hereafter called gradient images) that describe the canopy variation in height and highlight the topmost crowns compared with in-between crown areas (Fig. 5a and b). The gradient product is used to compute a binary image calculated as a function of a threshold that delineates the areas with the highest probability of representing a crown. However, our pixel-based approach produces many unrealistic crowns due to complex forest structure and highly overlapped crowns (Fig. 5c).
b) The OBIA approach was designed to remove the objects with unrealistic features. We carry out a connected component segmentation approach that transforms the binary image into a collection of objects from which we can calculate various crown characteristics

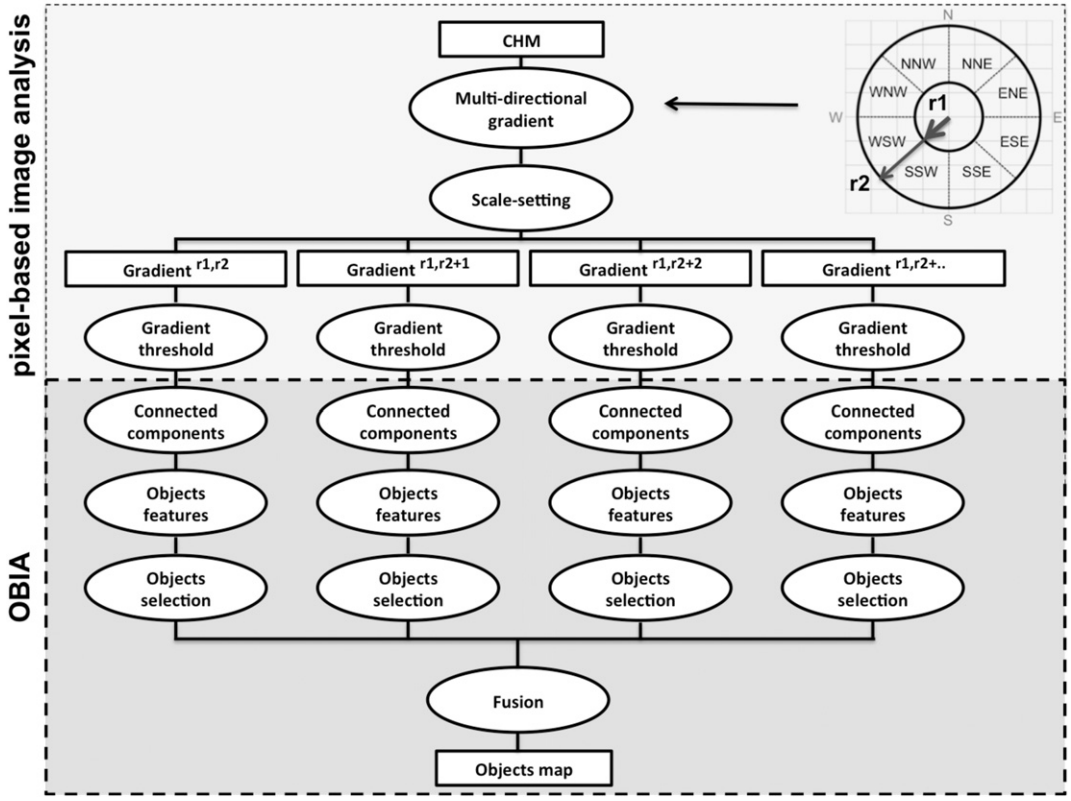

Fig. 4. Workflow of the CHM-based 2D individual crowns extraction (Section 3.2.1). OBIA stands for Object-Based Image Analysis. Image on the top right represents the multi-directional gradient filter composed of a circle (with diameter r1) and a concentric annulus (with diameter r1 and r2). Multi-scale gradient images are calculated by varying r2.

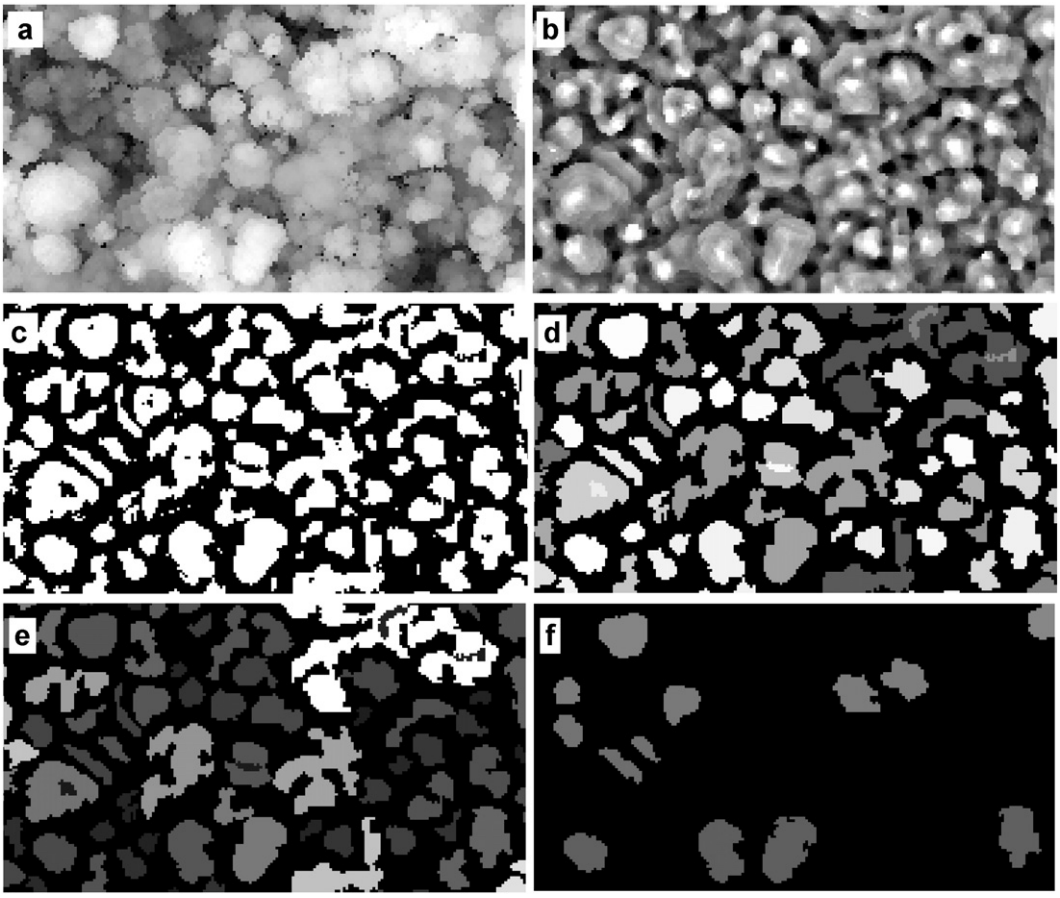

Fig. 5. Example of the 2D individual crowns extraction method over a given area (100 m × 200 m). a) Canopy height model, b) multi-directional gradient image calculated using Eq. (2) with r1 = 2 m and r2 = 8 m, c) binary image (white pixels = objects and black pixels = background), d) compactness of the objects, e) crown ratio of the objects and, f) objects that have been selected for the scale defined by r1 and r2. Brighter pixels correspond to higher values in b), d) and e).

such as crown area and crown shape (Fig. 5d and e). It allows selecting the individual crowns that follow the assumptions 2) and 3) listed here above (Fig. 5f). Finally, we merge the objects (i.e. the crowns) obtained through the multi-resolution analysis into a single individual crown map.

In the following, we explain the mathematical formulation of our workflow shown in Fig. 4. Let C and $C'_{r1,r2}$ represent the CHM and the CHM gradient images, respectively. The latter is calculated using the multi-directional gradient filter that is composed of a circle, with diameter $r1$, and a concentric annulus with diameter $r1$ and $r2$ such that $r1 < r2$ (top right of Fig. 4). Let I_{r1} and $O_{r1,r2}$ be the subset of C composed by pixels that are covered by the circle and the annulus, respectively. Furthermore, $O_{r1,r2}$ is divided into eight subsets ($O^d_{r1,r2}$) that are defined according to the secondary-intercardinal directions d = {NNE, …, NNW}. Therefore, $C'_{r1,r2}$ is calculated using:

$$C'_{r1,r2} = \frac{mean\left(P^d\right)}{\left|\left(max\left(P^d\right) - min\left(P^d\right)\right)\right|}, \quad (2)$$

$$with\ P^d = \left\{median(I_{r1}) - median\left(O^d_{r1,r2}\right)\right\}, for\ d = \{NNE, \ldots, NNW\})$$

where P^d is a set composed of eight elements, each one representing the gradient between the inner circle pixel values and the annulus pixels according to the eight predefined directions, and |.| represents the modulus.

Therefore, high values mean that the area covered by the inner circle is higher than the outer circle area for all eight directions, i.e. the filter was located near the summit of a concave downwards area that is likely to correspond to an ITC (brighter pixels in Fig. 5b). Accordingly, the values of $C'_{r1,r2}$ decrease as long as the filter applies to pixels closer to the crown boundary and are negative for pixels located in-between crowns. The parameters $r1$ and $r2$ define the extent of the areas that will show up brighter or darker in the gradient image: wider filters are adapted to enhance large crowns whereas narrow filters capture small crowns. The multi-scale analysis is carried out by setting $r1 = 1\ m$ and varying the size of the outer circle ($r2 = 3, 4, \ldots 9\ m$) in order to extract ITC of different sizes.

A gradient threshold (thr) is used to calculate a binary image ($B_{r1,r2}$, Fig. 5c) that represent the convex downwards areas with the highest probability to characterize isolated crowns:

$$B_{r1,r2} = 1_{\left\{C'_{r1,r2} > thr\right\}} \quad (3)$$

Where $1_{\{.\}}$ represents the identity function that sets the pixels to the value of one if the corresponding pixel in $C'_{r1,r2}$ is higher than thr and to zero otherwise. In this work we use $thr = 0.1$. However, due to the complex clumping tree patterns and high crown overlapping in tropical forests, our gradient-based method delineate not only ITC but also groups of trees, which in turn may negatively impact the establishment of a reliable allometric equation (Fig. 5c).

The OBIA has been designed to discard clusters of pixels corresponding to unrealistic tree structure. First, a 8-connected component segmentation is used to calculate the objects on the binary image $B_{r1,r2}$

(Samet & Tamminen, 1988). The selection of the realistic individual crowns is based on two attributes: the compactness and the crown ratio (Fig. 5d and e, respectively). The first one is defined as the quotient of the area of the object by the area of the smallest ellipse that encloses it, whereas the second one is the ratio of the object width to the object height. Both the area and the width were calculated by means of a C++ open source code based on the ITK (Insight ToolKit) library used to manipulate objects (Lehmann, 2008). Conversely, the height of the objects is calculated by averaging the pixels of the CHM that are covered by the delineated crown. We remove all objects with compactness less than or equal to 0.75 and with crown ratios outside the 0.4–0.6 range (Fig. 5f). The crown compactness is set to a conservative value because we focus on the objects with the highest probability to correspond to an individual crown with little interest in attaining a high detection rate. Similarly, the crown ratio range is conservative as well. On the one hand, the value of 0.6 has been chosen in order to remove objects with unrealistic high values that often correspond to single trees that have been segmented together with two or more adjacent crowns (Fig. 5c). This value agrees with the ground measurements in BCI suggesting that less than 6% of the trees have crown ratios higher than 0.6 (Bohlman & O'Brien, 2006). On the other hand, according to the ground measurements, the crown ratio of 70% of the trees is less than 0.4, which means that the selected crown ratio range discard many trees and we focus on the trees with high crown ratios for each forest height layer. This choice was made based on several simulations and comparisons with ground observations that led us to conclude that the bandwidth model is sensitive to the crown volume under-estimation. In fact, the AMS3D is more robust when the bandwidth model is calibrated as a function of the trees with higher crown ratios for a given forest height because they are more difficult to model due to the fact that they are more prone to display crowns with atypical shapes (e.g. crowns characterized by more than one tree top). On the contrary, the AMS3D efficiently extract trees with small crown ratios because they follow standard shapes (e.g. conical, ellipsoidal) and their leaves and branches are much more clustered.

Finally, the 2D individual crown maps are calculated by merging all objects generated from the multi-scale approach (Fig. 4). Although, both the tree height and crown width of the ITC could be directly retrieved from the 2D individual crowns map, no information on crown depth can be extracted directly from this analysis. For that purpose, we overlap the referred map showed in Fig. 5f to the lidar point cloud in order to compute the 3D ITC samples illustrated in Fig. 6. In the following we explain the method to estimate 3D crown metrics, both crown width and crown depth, from these samples.

3.2.2. Point cloud-based 3D individual crowns samples extraction

Tree crown size cannot be directly retrieved for the 3D ITC samples because in theory, they may contain lidar points reflected by other vegetation features such as dominant and co-dominated trees in the structure (Fig. 6). We model different layers of vegetation by fitting a sum of Gaussian functions to their vertical profile in order to characterize topmost crowns that correspond to the highest Gaussian curves out of the many that can result from this analysis (upper panels in Fig. 6).

First, a 1-meter bin size frequency histogram (green line in Fig. 6) is generated for each one of the 3D ITC samples from the corresponding lidar points. Then, we applied a Gaussian kernel with a variation equal to 1 and a radius of 2.5 to the histogram in order to calculate a smoother vertical profile (black dotted lines in Fig. 6). This Gaussian filter intends to better characterize the vertical profile of individual crowns by overcoming the limitation of the lidar in characterizing the crown base height of trees (Ferraz et al., 2012; Popescu & Zhao, 2008). For instance, the minimum separable distance between consecutive lidar points generated from the same lidar pulse, which is close to 2–3.5 m for most of commercial devices (such as the Optech ALTM 3100) contribute to this limitation (Popescu & Zhao, 2008; Ussyshkin & Theriault, 2010). We found that the smoothed histogram better models the vertical profile of vegetation because the noisy nature of the original 1 meter histograms could lead to the underestimation of the topmost crown height (e.g. Fig. 6a).

Therefore, the smoothed histogram is decomposed using a sum of Gaussian functions (gray dashed lines in Fig. 6, Mallet et al., 2010). The expected value (μ) and the standard deviation (σ) of the topmost Gaussian curve provide information on the characteristics of the crown of interest, namely its crown base height (CBH):

$$CBH = \mu - 3\sigma \tag{4}$$

where μ corresponds to the mean height of the topmost crown (red dashed line in Fig. 6) and the value of 3σ has been chosen so that almost 100% (99.7%) of the lidar points that give rise to the Gaussian curve are taken into account for the CBH calculation (blue dashed line in Fig. 6). However, the sum of Gaussian functions was robust to detect the expected values but it was unable to detect the true shape of some tree crowns due to complex frequency histograms. We selected the Gaussians corresponding to the highest expected value and with a reliable standard deviation associated. Indeed, for the sake of computation time, Gaussians with a standard deviation that meet $3\sigma < 1\ m$ or $2 \times 3\sigma > 0.8 \times TH$; where TH stands for tree height; were removed beforehand and not considered to calculate the CBH of the 3D ITC samples because they are obvious miscalculations of the sum of Gaussians approach (Eq. 4). Then, the points lower than CBH are removed to isolate the topmost crown. The TH is set to the height of the highest lidar point, whereas CD is the difference between the height of the lowest lidar point and TH. Finally, all individuals for which the tree height-crown depth ratio is not within the range $0.4 < \frac{CD}{TH} < 0.8$ are removed from the dataset. The motivation for selecting only the trees crowns within this range is similar to reason for the removal of 2D individual trees (Section 3.2.1). On the one hand, the purpose of the higher threshold is to remove unrealistic trees since according to ground measurements over BCI less than 6% of the trees have crown depth ratios higher than 0.8 (Bohlman & O'Brien, 2006). On the other hand, the lower threshold was set to 0.4 because the AMS3D produces better results if the bandwidth model is defined as a function of the trees with biggest crown size for a given forest height (please refer to the paragraph before the last one of Section 3.2.1 for additional details).

Finally, for the CW calculation the points from the topmost crown were first projected into the x-y plane and the corresponding smallest enclosing ellipse calculated using an algorithm from the open source C++ library CGAL (The CGAL Project, 2015). The CW equals to the mean of the corresponding minor and major axis.

3.2.3. Lidar-derived tree size allometry

Estimates on CW and CD calculated here above from the 3D ITC samples are plotted against TH in order to establish local allometric equations for bandwidth model calibration purposes. In the module called *Tree size allometry* of Fig. 2, we show an example that shows the TH-CW and TH-CD allometries represented by a green and orange line, respectively. Ground measurements campaigns over BCI and other tropical regions suggest there is a linear relationship between TH and both CD and CW (Bohlman & O'Brien, 2006; Goodman, Phillips, & Baker, 2013; Ploton et al., 2015). Accordingly, we developed linear regressions to calculating the bandwidth model in both horizontal

$$w^s(X_i) = s^s \times z_i \tag{5}$$

and vertical dimensions

$$w^z(X_i) = s^z \times z_i \tag{6}$$

where s^s and s^z correspond to the slope of the TH-CW and TH-CD linear allometric equations, respectively. Note that, the crown size allometric models were forced to cross zero to insure that for zero height, the crown diameter remain zero. Thus, for a given lidar point with coordinates $X_i = (x_i, y_i, z_i)$, we defined a 3D kernel (i.e. a cylinder as show in

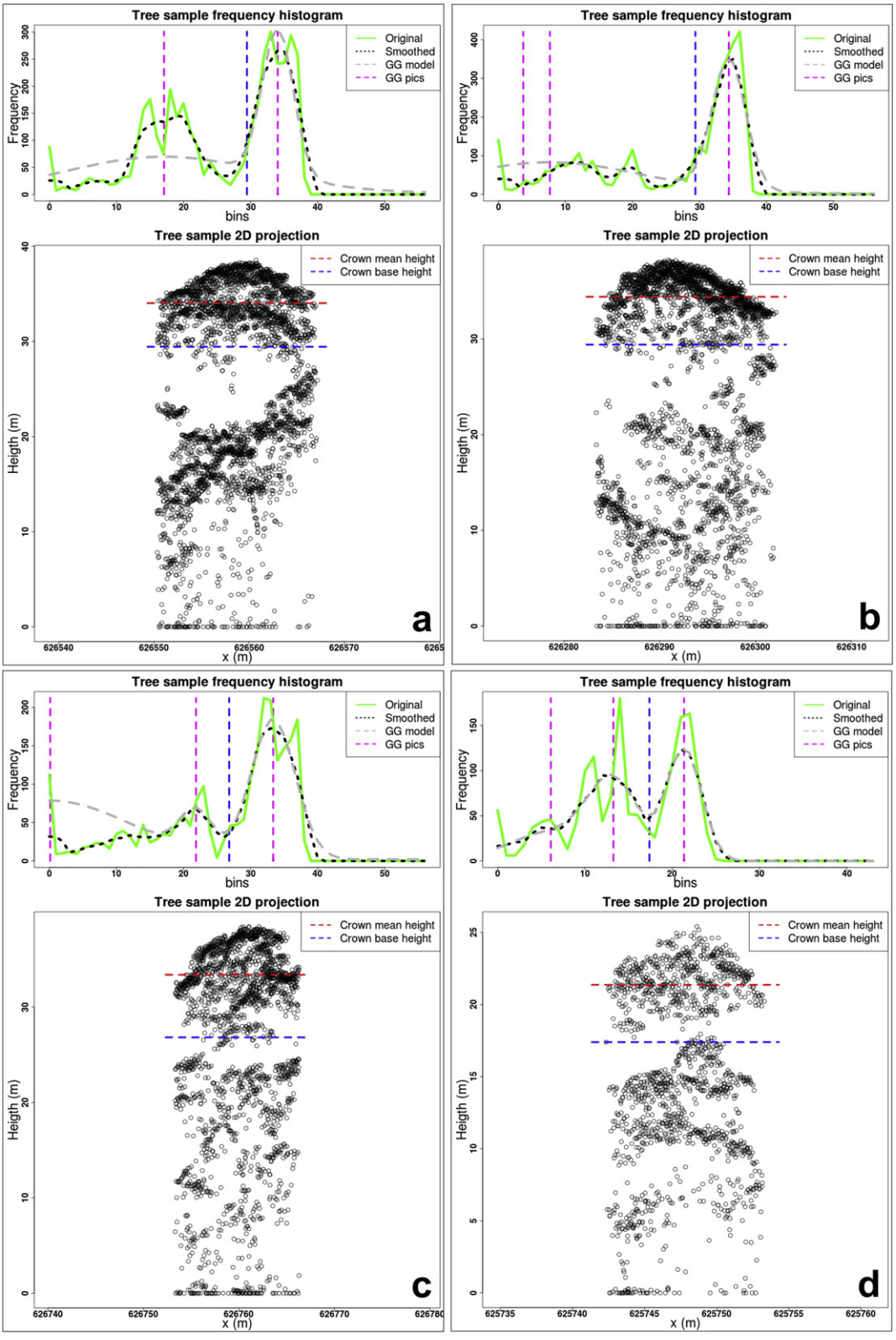

Fig. 6. Analysis of the 3D ITC samples to estimate the crown base of trees in order to remove underneath vegetation points. The panels on the top represent the 1 meter bin frequency histograms calculated from the lidar points (green lines), a smoother histogram calculated using a Gaussian filter (black dotted line), the fitted sum of Gaussian function (gray dashed lines), the position of the expected values (magenta dashed lines) and, the crown base height (blue dashed lines) calculated according to Eq. (4). The bottom panel shows the mean crown height (dashed red line, which is assigned to the highest expected value) and the crown base height (dashed blue line) along with the lidar points of the 3D ITC samples. (For interpretation of the references to color in this figure legend, the reader is referred to the web version of this article.)

Fig. 3) with diameter and height calculated from the horizontal and vertical bandwidths respectively (Eqs. (5) and (6)). An illustration is shown in the *Bandwidth model* module of Fig. 2.

3.3. Validation and uncertainty analysis

For validation of the results, we could not directly compare the AMS3D outputs such as tree height or crown size due to the lack of ground observations (Section 2.1). The ground data on individual tree height and crown size used in this paper for developing allometric relationships were measurements from almost 20 years before the lidar data acquisition. Because of changes in tree size over this long period, it was not feasible to locate and compare the crown size and height with the lidar data.

Instead, we compared the aboveground biomass (AGB) estimates from lidar tree height and crown size to ground-estimated AGB for trees with a diameter at breast height (DBH) >10 cm. The field-derived reference data is calculated by means of a commonly used allometric equation that estimates AGB on an individual tree-basis as a function of wood density (WD), DBH and tree height (TH, Eq. (7) in Table 2, Chave et al., 2005). The WD, which is a species-specific variable is set to a constant equal to the basal-area-weighted wood density for the entire 50 ha plot as $\overline{WD} = 0.5302$ kg m^{-3}. The assignment of the actual wood density to every tree would imply the prior identification of the tree species that is not here considered for the lidar estimation of biomass. To use the Chave et al. (2005) allometry to estimate AGB, we estimate TH of all trees from TH-DBH relationship showed in Eq. (12) inside Table 2 that have been calculated by Meyer et al. (2013) using the field measurements of 1604 sample trees in the plot (Bohlman & O'Brien, 2006).

Field-derived AGB is compared to lidar estimates by means of two different techniques that differ in the way they distribute the ABG throughout the space. This study allows assessing the errors associated with the so-called edge effect. In the first, which is the standard one and it is here called the stem-localized approach; the AGB of individual trees is allocated to a single location, i.e. to the coordinates of the stems (Section 3.3.1). The second one is called crown-distributed approach because the individual tree AGB is uniformly distributed along the crown (Section 3.3.2, Mascaro, Detto, Asner, & Muller-Landau, 2011).

3.3.1. Assessment of stem-localized aboveground biomass

The field-based AGB estimations are here compared to four different lidar-derived AGB models, which are established by means of two different approaches. In the first one, three out of the four models are established using the metrics derived from the 3D clusters provided by the AMS3D that can be used to estimate TH, CA, and CV (Eqs. (8)–(10), Table 2). The fourth approach is an existing method in which the model is derived from a metric called top of canopy height (TCH) that is calculated by averaging a CHM according to a given area (Asner & Mascaro, 2014).

Regarding the AMS3D-based models, 3D clusters have been modeled using a convex hull to estimate both CA and CV, whereas TH was assigned to the highest lidar point within the referred clusters (please refer to introduction of Section 3). Eq. (13) has been derived using the field data described in Bohlman and O'Brien (2006) to feed Eq. (10) because the AMS3D is unable to provide measurements on the DBH of trees (Table 2). In fact, Eq. (10) emulates Eq. (7) in order to assess how well the AMS3D metrics along with locally calibrated allometric models describe the AGB variability. In the TCH-based approach, we use a model relating AGB to TCH at the plot scale (Eq. (11), Table 2). Because the TCH needs to be related with AGB using field data, the resolution of the AGB maps depends on the plot inventory available. This model is shown to explain the AGB variability over different tropical forest environments (Asner & Mascaro, 2014) and, therefore, it can be used to examine any improvements of our individual tree-based method.

We examine the aptitude of AGB models M_1, M_2, M_3 and M_4 to capture the variance in AGB by comparing their results to reference field-based AGB estimates calculated using Eq. 7. The accuracy of the lidar-based models is evaluated using the coefficient of variation (R^2) and the root mean square error (RMSE) of the linear models AGB_{l1}, AGB_{l2} and AGB_{l3}, and of the power-law model AGB_{tch} (Table 2). Additionally, the regression coefficients (a_1, a_2, a_3, a_4, and α) of the later models allow us to investigate the magnitude of the correction needed in models M_1, M_2, M_3 and M_4 to properly estimate biomass. A regression coefficient of 1 would mean that no correction is needed and therefore models M_1, M_2, M_3 and M_4 could readily replace Chave et al. (2005) AGB allometry. Similarly, a regression coefficient different from 1 but constant across different study sites would mean that Chave et al. (2005) AGB allometry could be replaced as well given that such correction was applied.

Table 2
Aboveground biomass models and field derived tree allometric models. Eq. (7) is applied to estimate AGB using field measurements; whereas the lidar derived AGB is estimated using Eqs. (8), (9), (10), and (11). Eqs. (12), (13) and (14) correspond to tree allometry derived using ground measurements. Eq. (7) calculates AGB in kg m^{-1} and $\overline{WD}$, *DBH*, *TH*, *CV*, and *CA* stand for basal-area-weighted wood density (kg m^{-3}), diameter at breast height (cm), tree height (m), crown volume (m^3) and crown area (m^2), respectively.

AGB field-based model (lidar individual tree-based approach) (Chave et al., 2005)		
$AGB_f = 0.0509 \times \overline{WD} \times \sum_{i=1}^{n} DBH_i^2 \times TH_i$		(7)
AGB AMS3D-based models (lidar individual tree-based approach)		
$AGB_{l1} = a_1 \times M_1$, where	$M_1 = \overline{WD} \times \sum_{i=1}^{n} CV_i \times TH_i$	(8)
$AGB_{l2} = a_2 \times M_2$, where	$M_2 = \overline{WD} \times \sum_{i=1}^{n} CA_i \times TH_i$	(9)
$AGB_{l3} = a_3 \times M_3$, where	$M_3 = 0.0509 \times \overline{WD} \times \sum_{i=1}^{n} DBH_i^2 \times TH_i$	(10)
AGB TCH-based model (lidar statistical area-based approach)		
$AGB_{tch} = a_4 \times \overline{WD} \times M_4^{\alpha}$, where	$M_4 = TCH$	(11)
Individual tree allometry derived using field measurements (Bohlman & O'Brien, 2006)		
$TH = 22.766 \times log_{10}(\text{DBH}) - 11.731$	Used to feed Eq. (7)	(12)
$DBH = 1.2025 \times TH + 0.1408 \times CA$	Used to feed Eq. (10)	(13)
$CA = 0.017 \times DBH^2 + 0.1408 \times DBH$	Used to calculate the crown-distributed AGB maps (Section 3.3.2)	(14)

All linear models are forced to cross the origin (zero) in order to comply with the assumption that AGB cannot be greater than zero when the tree metrics are zero. This assumption is specially valid in our study area because mature forests at 1ha scale all have high biomass (160–425 Mg ha^{-1}) with no values close to zero causing the lidar biomass model to be unstable or spurious. Following Asner and Mascaro (2014), the model based on the metric M_4 is assumed to follow a power-law and is derived using an ordinary least squares technique. The AGB models showed in Table 2 are established at four different scales: 1ha, 2.25ha, 4ha and 6.25ha. It is well known that a general reduction in prediction error (RMSE) with larger plots is expected due to spatial averaging of errors (Goetz & Dubayah, 2011). However, since M_1, M_2, and M_3 are calculated as a sum of ITC-based values, the multi-scale analysis allows to investigate whether our approach systematically under- or over-estimate the ITC metrics. For instance, in the case a systematic bias in regarding the tree density estimation from the ITC method, the regression coefficients (a_1, a_2, a_3) would significantly differ depending on the spatial resolution. The behavior of coefficients a_4 and α will determine whether the model AGB_{M4} is scale dependent as well.

3.3.2. Assessment of crown-distributed aboveground biomass

Finally, we investigate the impact of the errors associated with the edge effect. The latter are mainly originated by 1) overhanging trees for which the stems are outside the plot boundary but their crowns or parts of their crowns are within it, and 2) GPS positional errors introduced by both lidar and field measurements, which can be significant due to poor GPS signal under dense tropical forest canopy. The impact of the edge effect on the AMS3D-based models is expected to be higher than on the TCH-based one. In fact, similarly to the field-based model (AGB_f), the AMS3D-based models (AGB_{l1}, AGB_{l2}, AGB_{l3}) place AGB in space according to the x and y coordinates of each tree. This can lead to discrepancies between the models due to the fact that field techniques locate trees according to the stem position whereas the AMS3D locate trees according to the center of the crown (Section 3.1). Conversely, in the TCH-based approach (AGB_{tch}) the model is established as a function of TCH, driven by laser beams reflected by the tree crowns rather than tree stems. Therefore, there is no rigid rule that determines if a tree is "in" or "out" and trees that are bisected at the plot edge can somewhat compensate for the edge effect.

To test the impact of the edge effect on the models, we follow the work of Mascaro et al. (2011) in which the individual tree AGB is uniformly distributed along the crown instead of allocating the AGB to a single location (i.e. to the x,y coordinates of the tree). It allows computing crown-distributed maps of ABG density at a given pixel resolution that we, in this work, set to 1 m. Regarding the field-derived map, the individual tree AGB is given by Eq. 7 whereas trees are located according to the surveyed stem coordinates. Moreover, the crowns are assumed to be a circle and its area is calculated using Eq. (14), which is derived using the data described in Bohlman and O'Brien (2006). In the AMS3D approach, three different crown-distributed AGB maps can be derived using separately models AGB_{l1}, AGB_{l2}, AGB_{l3} (Table 2). Therefore, the AGB is calculated using Eqs. 8–10 using the scaling parameters (a_1, a_2, a_3) found in the previous section (Section 3.2.1) and setting $n = 1$ since we are calculating individual tree AGB. Finally, for mapping purposes, the crowns are assumed to be a circle and its radius is calculated from the individual tree CA. Because the AGB_{tch} only maps the AGB at coarser scales (usually > 1ha), none of the stem-localized or the crown-distributed maps can be generated from its outputs.

4. Results and discussion

In Section 4.1 we assess the reliability of the method that establishes local tree allometric models from the 3D individual tree crown (ITC) samples. The allometry is used to calibrate the bandwidth model required by the AMS3D to decompose the entire lidar point cloud into ITC, which allows to estimate the crown size and tree density along with the tree size that are used to establish aboveground biomass (AGB) models (Section 4.4). The latter are compared to field measurements at four different spatial scales (1ha, 2.25ha, 4ha and 6ha, Section 4.3). Finally, the impact of the edge effect on the 1ha AGB models is assessed using crown-distributed AGB maps (Section 4.4).

4.1. Bandwidth model estimation

The bandwidth model is defined by the tree height-crown size allometry calculated using the lidar-derived 3D ITC samples (Section 3.2.3 and Fig. 2). Fig. 7 shows the tree height (TH) plotted against crown width (CW) and crown depth (CD) that is used to calculate the allometric linear models over BCI using Eqs. (5) and (6) (Section 3.2.3). It shows that our technique provides much more measurements on CW than on CD because the sum of Gaussian functions was unable to detect the true form of some vertical profiles of 3D ITC samples due to complex histogram frequencies (Section 3.2.2). However, we assume that the number of measurements is enough to establish a robust tree height-crown size relationship and the discrimination between topmost and underneath crowns is improved by applying AMS3D technique that uses the 3D lidar point cloud instead of to a 2D frequency histogram. Furthermore, the effect of the lower crown size ratio threshold ($0.4<\frac{CW}{TH}<0.6$ and $0.4<\frac{CD}{TH}<0.8$) is readily shown in Fig. 7, which means that the image based approach found many trees with a lower crown ratio than 0.4 that were subsequently removed from the analysis. It is important to note that these trees were removed because we defined the bandwidth model to be calibrated as a function of the trees with the higher crown ratios within a given forest layer. This is due to the fact that the AMS3D method is more sensitive to such trees because they are more prone to have atypical shapes compared with trees with smaller crown ratios (Section 3.2.1). Fig. 7 also shows that the multi-scale analysis dedicated to delineate crown boundaries from the CHM data (Fig. 5) covers the entire range of tree size from almost10 m to 45 m height, and crown size from about 5 m to 25 m in width or depth. This range corresponds to approximately all trees with DBH > 10 cm.

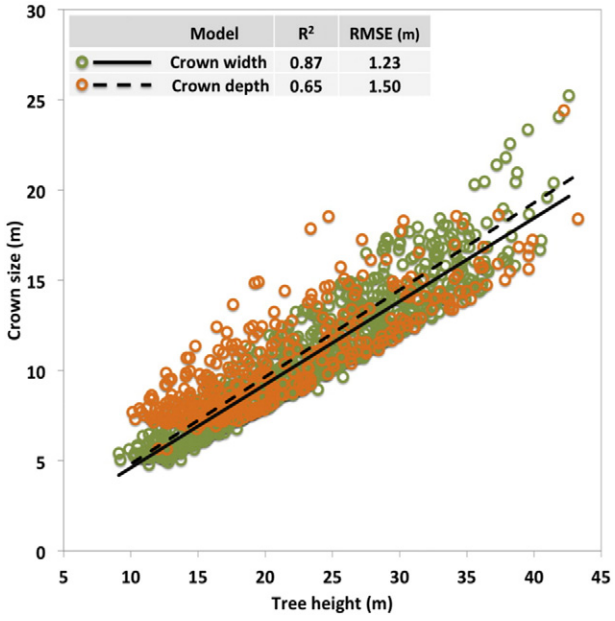

Fig. 7. Allometric models for crown width (Eq. (15)) and crown depth (Eq. (16)) derived from the lidar 3D ITC samples measurements and the corresponding coefficient of determination (R^2) and root mean square error (RMSE).

Therefore, data shown in Fig. 7 is used to calculate the diameter and the height of the 3D kernel from the TH-CW and TH-CD allometry, respectively. The linear models represented by Eqs. (5) and (6) are fitted to the data to define the bandwidth model for the BCI study site:

$$w^s(X_i) = 0.4612 \times z_i \quad (15)$$

and

$$w^z(X_i) = 0.4812 \times z_i \quad (16)$$

Thus, for a given lidar point with coordinates $X_i = (x_i, y_i, z_i)$, we defined a 3D kernel (i.e. a cylinder as show in Fig. 3) with diameter and height calculated from the horizontal and vertical bandwidths respectively (Eqs. (15) and (16)). The coefficient of determination R^2 and the root mean square error (RMSE) of the models were calculated for crown width ($R^2 = 0.87$; RMSE = 1.23 m) and crown depth ($R^2 = 0.65$; RMSE = 1.5 m, Fig. 7). The results show that on the average the crown depth (CD) of the 3D ITC samples is slightly larger than the crown width (CW), which agrees with the field measurements carried out by Bohlman and O'Brien (2006).

4.2. Distribution of individual tree size

Eq. (1) is fed by both Eq. (15) and Eq. (16) in order to define the bandwidth required by the ASM3D to decompose lidar point clouds into 3D clusters that represent ITC. Fig. 8a and b shows the 50ha plot in BCI comprising 5,409,601 points (10.8 pt/m^2 in average) that took nearly 11.7 h to process using the AMS3D algorithm implemented in C++.

We extract from the AMS3D product (Fig. 8a) the individual tree location, tree height (TH), crown area (CA), and crown volume (CV) by modeling each 3D cluster using a convex hull (Section 3.3.1). The lack of ground measurements on tree height and crown size prevents a quantitative assessment concerning the ability of the AMS3D to capture the spatial variability regarding the referred metrics (Section 3.3). Nevertheless, Fig. 8c and d indicate that the AMS3D is able to correctly estimate the size-abundance relationships for TH and CA, respectively. In fact, there is limited ground-based analysis on those relationships over tropical regions, but they report probability density functions with shapes similar to the ones shown in Fig. 8c and d. In particular, tropical tree height distributions are characterized by a right-skewed distribution with the peak corresponding to mid-range trees (Kent, Lindsell, Laurin, Valentini, & Coomes, 2015; Shimizu et al., 2014), which is around 10–15 m over the BCI 50ha plot according to the AMS3D (Fig. 8c). Unlikely, the individual CA size distribution (Fig. 8d) shows a probability density function similar to the DBH size-abundance relationship reported in different sites, which are characterized as either negative exponential or power law functions (Coomes, Duncan, Allen, & Truscott, 2003; Muller-Landau et al., 2006; White, Ernest, Kerkhoff, & Enquist, 2007). The fact that former studies suggest that there is a linear relationship between DBH and CA (Bohlman & O'Brien, 2006; Goodman et al., 2014; Ploton et al., 2015) suggests that the AMS3D is able to estimate the CA probability density function correctly. However, the assessment of those relationships and many others tropical ecological studies have been limited due to the lack of crown size measurements over space and time. The AMS3D product can significantly contribute for such studies with focus on the largest trees because their size-abundance relationship deviate from simple exponential or power law models (Coomes et al., 2003; Enquist & Niklas, 2001; Muller-Landau

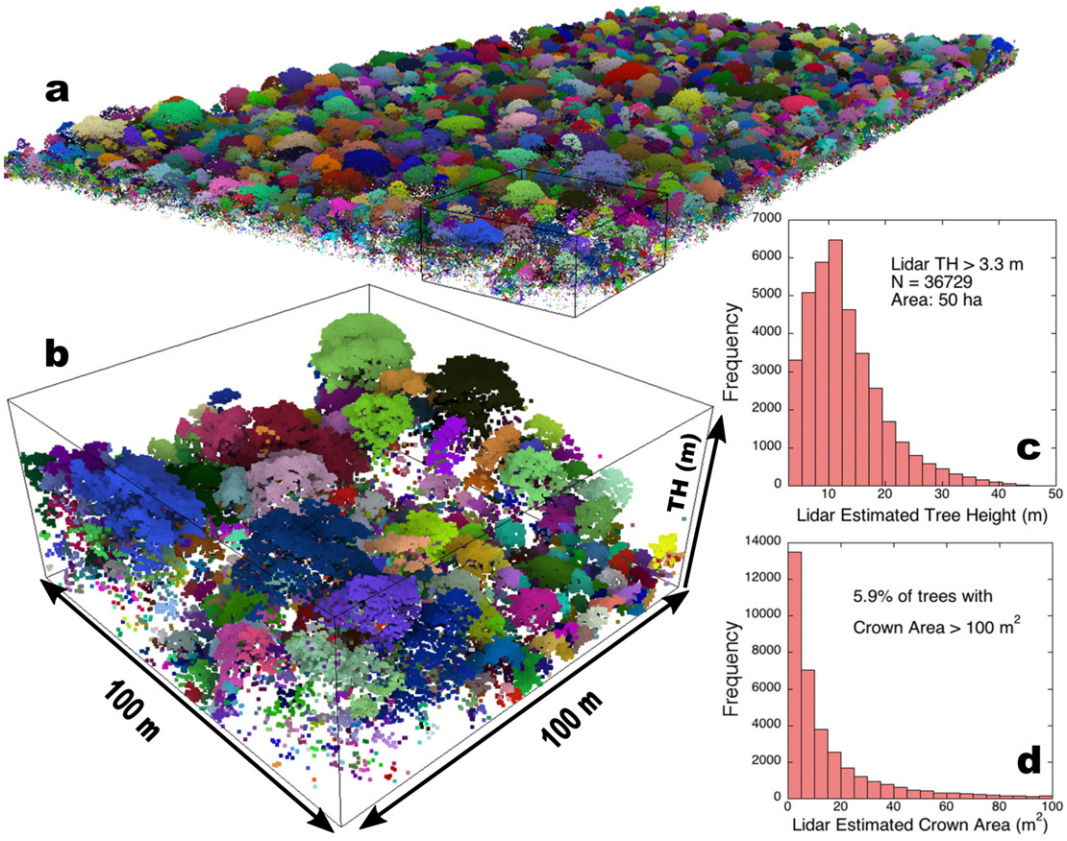

Fig. 8. AMS3D map representing individual crowns over a) the 50ha plot in BCI, b) a zoomed sample area of 1ha with colors randomly assigned to the AMS3D clusters that correspond to individual trees and, distribution of lidar derived individual c) tree height and d) crown area with about 5.9% of trees with crown area > 100 m^2 not shown in the graph for better visualization of results. (For interpretation of the references to color in this figure legend, the reader is referred to the web version of this article.)

et al., 2006) and, the lidar is better suited to measure their crown size than ground techniques. Mapping and tracking the largest individual trees is particularly important because they comprise most of the biomass and highly impact the forest structure dynamics by creating gaps and death (Chambers et al., 2007).

4.3. Stem-localized above-ground biomass

The AGB models shown in Table 2 were established at four different spatial resolutions: 1ha, 2.25ha, 4ha and 6.25ha. Because the plots are adjacent and do not overlap, models were defined as a function of 50 (1ha), 18 (2.25ha), 10 (4ha) and 8 (6.25ha) points, respectively (Fig. 9). Regarding the 1ha models, Table 3 shows that AGB_{tch} explains 68% of the variation in AGB, slightly better than the best AMS3D-based models (AGB_{l2}, with $R^2 = 0.63$) and it clearly outperforms AGB_{l1} ($R^2 = 0.46$). The root mean square error (RMSE) shows a similar trend: AGB_{l2} compares with AGB_{tch} whereas AGB_{l3} has lower predictive power but better than AGB_{l1} (13.8%, 12.5%, 15% and 16.9% of field-derived AGB, respectively). In Section 4.4 we show that all models improve predictive power when edge effect is reduced.

As for the multi-scale analysis, the predictive power increased with decreasing spatial resolution for all models. For instance, from 1ha to 6.25ha, the RMSE of observed AGB as predicted by AGB_{l1} decreases from 40.42 to 12.08 Mg ha^{-1}. Such a result was expected for the AGB_{tch} model due to spatial averaging of errors (Section 2.4, Mascaro et al., 2011; Zolkos et al., 2013) but it was unclear if the AMS3D-based models would behave similarly. Unlike AGB_{tch}, which is based on the top-of-canopy height (TCH), all AGB_{l1}, AGB_{l2} and AGB_{l3} models rely on the summation of individual tree characteristics and the multi-scale analysis shows that the AMS3D is unbiased regarding the estimation of the crown features (CV, CA and TH) as well as regarding the tree density, i.e. it does not systematically under- or over-estimate the number of trees. In addition, the improvements in terms of RMSE with decreasing spatial resolution are greater for the AMS3D-based models than for the AGB_{tch} model. The AGB_{tch} model performs better at 1ha and slightly better at 2.25 ha due to edge effect, but the other models start outperforming the latter at the 4ha and 6.25ha scales. Finally, our results show that, contrary to the AMS3D-based models, the AGB_{tch} is scale dependent. Indeed, the estimated slopes a_1, a_2 and a_3 show little variance compared with both α and a_4 when the models are established at different resolutions (Table 3). We believe that this is due to the fact that the AMS3D-based models are derived from the summation of fine scale metrics and not from averaged values (i.e. the TCH) according to a given area.

Comparison of the AMS3D-based methods with each other shows that in general AGB_{l2} outperforms both AGB_{l1} and AGB_{l3}. It leads to better results in terms of both R^2 and *RMSE* with the exception of the 6.25-ha models. Surprisingly, the calibration parameter of AGB_{l2} turns out to

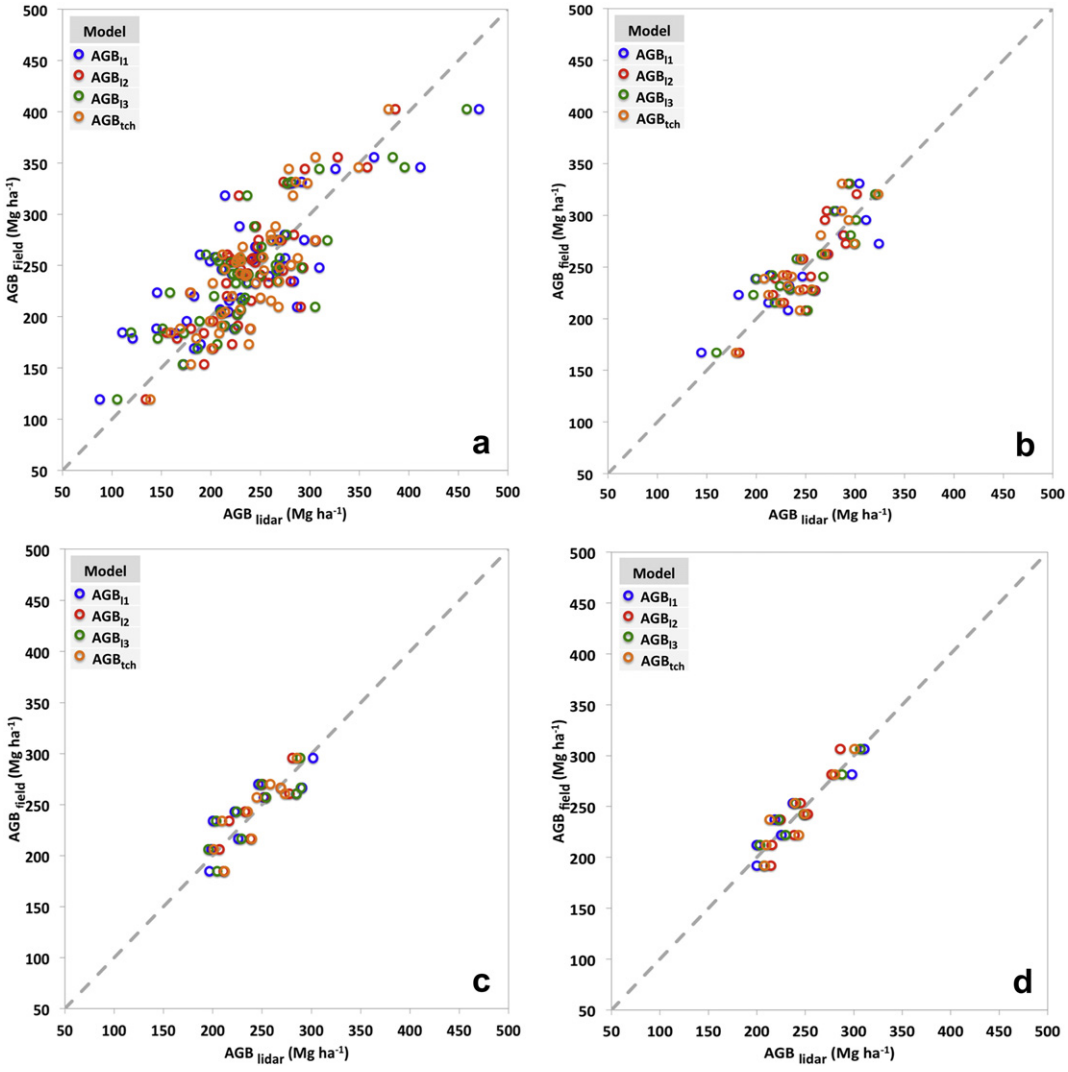

Fig. 9. Field- vs. lidar-derived AGB in the 50ha plot in BCI for a range of spatial resolutions: a) 1ha, b) 2.25ha, c) 4ha and d) 6.25ha. Details on the models and corresponding results are shown in Table 3.

Table 3
Regression model parameters and corresponding errors according to Table 2.

	AGB_{l1}			AGB_{l2}			AGB_{l3}			AGB_{tch}			
	R^2	RMSE	a_1	R^2	RMSE	a_2	R^2	RMSE	a_3	R^2	RMSE	α	a_4
1 ha	0.46	40.42 (16.9%)	0.14	0.63	33.62 (13.8%)	0.96	0.56	36.51 (15%)	0.75	0.68	30.53 (12.5%)	1.54	1.71
2.25 ha	0.64	24.41 (9.7%)	0.15	0.72	21.59 (8.5%)	0.98	0.68	23.3 (9.2%)	0.76	0.76	20.11 (7.96%)	1.83	0.68
4 ha	0.64	19.1 (7.8%)	0.15	0.75	15.8 (6.5%)	0.97	0.65	18.9 (7.8%)	0.76	0.72	15.93 (6.5%)	1.6	1.4
6.25 ha	0.88	12.08 (5%)	0.14	0.84	14.1 (5.8%)	0.97	0.91	10.33 (4.2%)	0.77	0.81	14.01 (5.8%)	1.88	0.57

be $a_2 \approx 1$, which indicates that the model is able to accurately estimate the AGB distribution at the absence of any field measurements for model calibration. In fact, we were expecting $a_3 \approx 1$ because AGB_{l3} emulates the field-based model AGB_f (Table 3). Nevertheless, a value of $a_3 \approx 0.76$ was found, which might mean that the TH-DBH allometric models that have been locally derived is not able to accurately capture the DBH variability from the TH measurements, especially for the largest trees that contribute the most to AGB estimates. This is due to the fact that large canopy trees in tropical forests do not accurately follow a TH-DBH model (Feldpausch et al., 2011; Muller-Landau et al., 2006). Moreover, the use of AGB_{l3} is limited to the few tropical areas where field measurements on both DBH and TH are available. Conversely, both AGB_{l1} and AGB_{l2} do not rely on any field measurements but only on tree metrics directly retrieved by the AMS3D. Consequently, these models better estimate the AGB at various scales because they accurately characterize the forest structure variability and outperform AGB_{l3}. Among the AGB_{l1} and AGB_{l2} models, the one based on crown area (CA) outperforms the model based on crown volume (CV) at all scales. Although no analysis has been made due to the lack of field measurements on CD, we believe that the AMS3D better extracts the CA than the CD because the topmost part of the crowns prevent the laser beam to reach the base of the crowns.

Furthermore, by estimating the CA and using it in the Chave et al. (2005) allometry to estimate AGB, we are providing a proxy for DBH in the model. There is limited data on the relationship between DBH and CA in tropical forests from ground measurements, but they all suggest a significant linear relationship between the two (Bohlman & O'Brien, 2006; Goodman et al., 2014; Ploton et al., 2015). Therefore, this indicates that our method is a reliable tool to estimate CA and it proves that the bandwidth model, which is locally calibrated using the tree size allometry derived from the lidar data, is able to depict the crown size variability in such a complex environment. Finally, due to the fact that the AMS3D is a self-calibrated approach, it is expected to successfully extract trees over different tropical environments.

4.4. Crown-distributed above-ground biomass

The impact of edge effect decrease with increasing spatial resolutions because the percentage of trees affected decreases as long as the ratio of plot length-to-area decreases. As a result, the crown-distributed analysis is carried out for the 1ha plots only since no significant edge effect impact is expected on the results for larger plot sizes. Therefore, the crown-distributed AGB density maps (1m resolution) shown in Fig. 10 calculated according to the methodology described in Section 3.3.2 had been aggregated to 1ha resolution AGB maps in order to compare the field-based model (AGB_f) to the lidar-based models (AGB_{l1}, AGB_{l2}, AGB_{l3}).

Although all the models slightly improved the results compared with the stem-located approach, the greatest improvements in RMSE have occurred within the AMS3D models: it decreases by 3.4%, 2%, 2.6% and 1.3% for AGB_{l1}, AGB_{l2}, AGB_{l3}, and AGB_{tch}, respectively (Fig. 11 and Table 3). Such a result shows that the impact of the edge effect is higher on the AMS3D-based models and that they perform equally well to the CHM-based one when such errors are reduced by means of the crown distributed approach.

Additionally, the crown-distributed AGB density maps highlight that the models map AGB differently. In the field-based model AGB_f, trees with the largest DBH clearly dominate the landscape in terms of AGB stocks and they can be easily recognized trough their sharp yellow contours in Fig. 10a (max = 178.4, mean = 24.2, σ = 23.8 kg m^{-1}). Because the field-based estimates are mainly driven by the DBH measurements, there is no direct relationship between AGB stock and crown size. In fact, by comparing the CHM (Fig. 1) to Fig. 10a one can conclude that AGB is not uniformly distributed in areas with high and closed canopy but is rather concentrated in one or two specimens located within those areas. Conversely, in the AGB maps based on CV estimates, there is a higher correlation between the areas showing denser AGB with the areas where the higher and closed canopy are located. The tree crown contours in yellow are not as sharp as in Fig. 10a and AGB is more uniformly distributed among the biggest trees in crown size (Fig. 10b, max = 139.6, mean = 23.1, σ = 17.8 kg m^{-1}).

Furthermore, AGB_{l2} produces density maps in which AGB is even more evenly distributed than the latest cases in which the individual trees that hold the most AGB are much more difficult to recognize (Fig. 10c, max = 118.9, mean = 24.7, σ = 14.5 kg m^{-1}). As a result, comparing Fig. 10b with Fig. 10c readily show that a few trees are dominating in terms of CV whereas a larger number of trees show similar CA sizes. Finally, the pattern of the map produced by the AGB_{l3} model is closely related with that one of AGB_{l1} (Fig. 10d, max = 199.6, mean = 24.1, σ = 18.7 kg m^{-1}). However, a speckle effect can be recognized in the AGB maps that correspond to high AGB concentrations in small regions of one to eight pixels in size. They mainly correspond to trees between 18 and 28 m high for which the AMS3D allegedly under-estimates their CA and therefore the AGB is allocated to just a few pixels. This effect could be removed by estimating the DBH of trees using CA alone instead of both TH and CA in Eq. (11), which gives much more importance to TH than to CA. Note that this effect only shows up over high resolutions AGB density maps and, according to Fig. 11, does not impact the analysis at coarser resolutions.

5. Conclusion

In this paper, we successfully apply a lidar-based method based on the 3D adaptive mean shift (AMS3D) technique to estimate individual tree size and density. The AMS3D relies on a single parameter called the bandwidth that is calibrated as a function of a local allometric model that is developed by automatic detection of isolated individual tree samples using the lidar data. Therefore, it is a self-calibrated approach that as the potential to successfully apply to diverse locations across tropical forests. By applying the AMS3D technique with adaptive bandwidth to lidar data, we shown that the approach accurately captures the variability of individual tree height, crown size, and tree

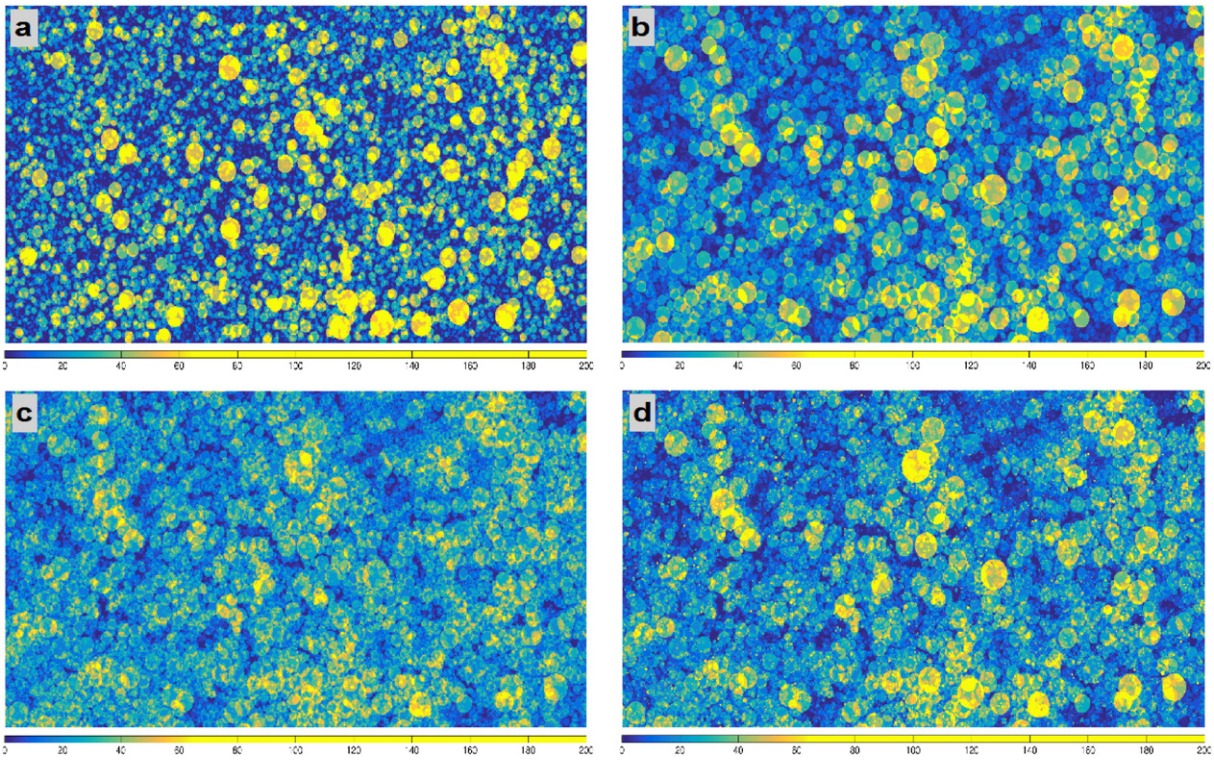

Fig. 10. Crown-distributed AGB maps for the 50ha CTFS plot (kg m^{-1}) derived from 1m resolution lidar, showing a) AGB_f, b) AGB_{l1}, c) AGB_{l2}, and d) AGB_{l3} (Table 3).

number density. These metrics were used to calculate aboveground biomass (AGB) and the results were validated over the 50ha CTFS plot in BCI. The predictive power of the AGB models derived from AMS3D-based structural information compare to the ground-estimated AGB at scales equal or greater than 1ha. Moreover, the multi-scale analysis shows that our ITC method is unbiased regarding the estimation of crown size and tree number density, i.e. does not systematically under- or over-estimate the tree number of trees. Our methodology has several advantages over conventional ground and lidar techniques:

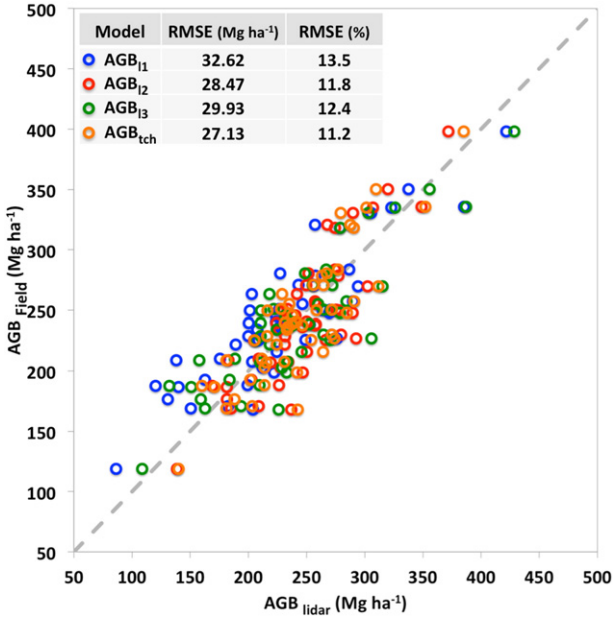

Fig. 11. Lidar- vs. field-derived of crown-distributed AGB in the 50-ha plot in BCI for 1ha plots. Details on the models and corresponding results are show in Table 3.

1) The ability to measure attributes of individual trees was limited to a few ground-based forest inventory plots that are not adapted to capture forest structure gradients at the landscape level and over inaccessible regions. Temporal sampling is restricted as well and there are local-scale difficulties measuring important biophysical variables such as tree height and crown size (Chambers et al., 2007). The AMS3D technique offers the first full 3D forest structure characterization in both vertical and horizontal dimensions at the individual tree level that was lacking in the framework of many applications such as light environment analysis, gap dynamics, and forest growth studies. Moreover, it has the potential of providing reliable information over space and time to refine existing demography and allometric models for simulating carbon dynamics of tropical forests (Antonarakis, Saatchi, Chazdon, & Moorcroft, 2011; Medvigy, Wofsy, Munger, Hollinger, & Moorcroft, 2009).
2) The AMS3D provides direct retrieval of individual tree metrics (e.g. tree density, tree height and crown size) that allow testing the hypothesis that lidar-based AGB models can be derived in order to replace or complement ground-based AGB models such as the one established in Chave et al. (2005). It would remove the need for collecting a large number of sampling plots (of about 1ha) required to locally calibrate the Canopy Height Model-based approach that have large uncertainty when used regionally or globally (Asner & Mascaro, 2014). In fact, our expectation is that the coeficcients of calibration of the AMS3D-based AGB models found in this work would not change significantly across different study sites. Assuming this a hypotheses, and tested true, the lidar-based AGB models would provide a universal approach to convert lidar crown size measurements into AGB without the need for ground sampling for calibration purposes.
3) Similarly to ground-based techniques, our approach provides estimates of AGB at the individual tree level by applying the Chave et al. (2005) allometric model. Due to the fact that the airborne lidar is not adapted to measure the DBH of trees, the latter has been replaced by metrics provided by the AMS3D such as crown area and crown volume. Results show that the best ASM3D-based model to

estimate AGB is achieved by replacing DBH^2 with crown area. It suggests that the crown area detected from lidar can be used as a proxy to replace DBH. In particular, regarding many large emergent trees, for which the field measurement of DBH may lead to large inaccuracies due to the presence of buttress, the lidar provides a more robust and accurate measurements of crown area (Chambers et al., 2007).

4) The AMS3D approach provides, for the first time, detailed information about the individual tree height and crown size, particularly for large and emergent trees that are irregular size and shapes and do not follow any specific growth allometric models (Muller-Landau et al., 2006). Quantifying the height and density of the large trees can readily provide an estimate of aboveground biomass with low uncertainty as tree height for large trees are difficult to measure in the field and contribute significantly to the biomass (Slik et al., 2013). Moreover, accounting for the crown size in the AGB allometry for the largest trees in a plot can significantly improve the AGB estimation (Goodman et al., 2014; Ploton et al., 2015). Additionally, mapping, measuring and tracking large trees offer additional benefits in understanding tropical forest dynamics at the landscape level because they highly drive the surrounding forest structure by creating gaps and death.
5) The AMS3D-derived tree size distribution creates a platform to develop new lidar remote sensing techniques at species level that can be used to quantify the taxonomic and functional diversity of tropical forests. By including high-resolution hyperspectral imagery along with the lidar point-cloud data, the object-oriented segmentation of species and their functional traits can be directly attributed to individual tree size (particularly the large trees), allowing for a complete characterization of tropical forest from remote sensing platforms.

Acknowledgments

António Ferraz's research was supported by an appointment to the NASA Postdoctoral Program at the Jet Propulsion Laboratory, administrated by Oak Ridge Associated Universities under contract with NASA (grant number NNH15CO48B).

References

Antonarakis, A., Saatchi, S., Chazdon, R., & Moorcroft, P. (2011). Using Lidar and Radar measurements to constrain predictions of forest ecosystem structure and function. *Ecological Applications*, *21*(4), 1120–1137. http://dx.doi.org/10.1890/10-0274.1.

Asner, G., & Mascaro, J. (2014). Mapping tropical forest carbon: Calibrating plot estimates to a simple LiDAR metric. *Remote Sensing of Environment*, *140*, 614–624. http://dx.doi.org/10.1016/j.rse.2013.09.023.

Asner, G., Mascaro, J., Anderson, C., Knapp, D., Martin, R., Kennedy-Bowdoin, T., ... Bermingham, E. (2013). High-fidelity national carbon mapping for resource management and REDD+. *Carbon Balance and Management*, *8*(1), 7. http://dx.doi.org/10.1186/1750-0680-8-7.

Asner, G., Palace, M., Keller, M., Pereira, R., Silva, J., & Zweede, J. (2002). Estimating canopy structure in an Amazon Forest from laser range finder and IKONOS satellite observations. *Biotropica*, *34*(4), 483–492.

Bohlman, S., & O'Brien, S. (2006). Allometry, adult stature and regeneration requirement of 65 tree species on Barro Colorado Island, Panama. *Journal of Tropical Ecology*, *22*(02), 123–136. http://dx.doi.org/10.1017/S0266467405003019.

Burman, H., & Soininen, A. (2004). *TerraMatch User's Guide*. Retrieved from http://www.terrasolid.fi/system/files/tmatch.pdf

Chambers, J., Asner, G., Morton, D., Anderson, L., Saatchi, S., Espírito-Santo, F., ... Souza, C. (2007). Regional ecosystem structure and function: Ecological insights from remote sensing of tropical forests. *Trends in Ecology and Evolution*, *22*(8), 414–423. http://dx.doi.org/10.1016/j.tree.2007.05.001.

Chave, J., Andalo, C., Brown, S., Cairns, M. A., Chambers, J. Q., Eamus, D., ... Yamakura, T. (2005). Tree allometry and improved estimation of carbon stocks and balance in tropical forests. *Oecologia*, *145*(1), 87–99. http://dx.doi.org/10.1007/s00442-005-0100-x.

Chave, J., Réjou-Méchain, M., Búrquez, A., Chidumayo, E., Colgan, M., Delitti, W., ... Vieilledent, G. (2014). Improved allometric models to estimate the aboveground biomass of tropical trees. *Global Change Biology*, *20*(10), 3177–3190. http://dx.doi.org/10.1111/gcb.12629.

Condit, R. (1998). *Tropical forest census plots: Methods and results from Barro Colorado Island, Panama and a comparison with other plots*. Springer-Verlag. http://dx.doi.org/10.1007/978-3-662-03664-8.

Condit, R., Engelbrecht, B., Pino, D., Pérez, R., & Turner, B. (2013). Species distributions in response to individual soil nutrients and seasonal drought across a community of tropical trees. *Proceedings of the National Academy of Sciences*, *110*(13), 5064–5068. http://dx.doi.org/10.1073/pnas.1218042110.

Coomes, D., Duncan, R., Allen, R., & Truscott, J. (2003). Disturbances prevent stem size-density distributions in natural forests from following scaling relationships. *Ecology Letters*, *6*(11), 980–989. http://dx.doi.org/10.1046/j.1461-0248.2003.00520.x.

Detto, M., Asner, G., Muller-landau, H., & Sonnentag, O. (2015). Spatial variability in tropical forest leaf area density from multireturn lidar and modeling. *Journal of Geophysical Research*, *120*(2), 294–309. http://dx.doi.org/10.1002/2014JG002774.

Enquist, B. J., & Niklas, K. J. (2001). Invariant scaling relations across tree-dominated communities. *Nature*, *410*(6829), 655–660. http://dx.doi.org/10.1038/nature02023.

Feldpausch, T. R., Banin, L., Phillips, O. L., Baker, T. R., Lewis, S. L., Quesada, C. a., ... Lloyd, J. (2011). Height-diameter allometry of tropical forest trees. *Biogeosciences*, *8*(5), 1081–1106. http://dx.doi.org/10.5194/bg-8-1081-2011.

Féret, J. B., & Asner, G. P. (2013). Tree species discrimination in tropical forests using airborne imaging spectroscopy. *IEEE Transactions on Geoscience and Remote Sensing*, *51*(1), 73–84. http://dx.doi.org/10.1109/TGRS.2012.2199323.

Ferraz, A., Bretar, F., Jacquemoud, S., Gonçalves, G., Pereira, L., Tomé, M., & Soares, P. (2012). 3-D mapping of a multi-layered Mediterranean forest using ALS data. *Remote Sensing of Environment*, *121*, 210–223. http://dx.doi.org/10.1016/j.rse.2012.01.020.

Ferraz, A., Mallet, C., Jacquemoud, S., Gonçalves, G. R., Tomé, M., Soares, P., ... Bretar, F. (2015). Canopy density model : A new ALS-derived product to generate multilayer crown cover maps. *IEEE Transactions on Geoscience and Remote Sensing*, *53*(12), 6776–6790. http://dx.doi.org/10.1109/TGRS.2015.2448056.

Goetz, S., & Dubayah, R. (2011). Advances in remote sensing technology and implications for measuring and monitoring forest carbon stocks and change. *Carbon Management*, *2*(3), 231–244. http://dx.doi.org/10.4155/cmt.11.18.

Goodman, R., Phillips, O., & Baker, T. (2013). *Data from: The importance of crown dimensions to improve tropical tree biomass estimates*. Dryad Data Repository: Ecological Applications. http://dx.doi.org/10.5061/dryad.p281g.

Goodman, R., Phillips, O., & Baker, T. (2014). The importance of crown dimensions to improve tropical tree biomass estimates. *Ecological Applications*, *24*(4), 680–698. http://dx.doi.org/10.1890/13-0070.1.

Hall, F. G., Bergen, K., Blair, J. B., Dubayah, R., Houghton, R., Hurtt, G., ... Wickland, D. (2011). Characterizing 3D vegetation structure from space: Mission requirements. *Remote Sensing of Environment*, *115*(11), 2753–2775. http://dx.doi.org/10.1016/j.rse.2011.01.024.

Hubbell, S., & Foster, R. (1983). Tropical rain forest: Ecology and management. In T. Whitmore, A. Chadwick, & A. Sutton (Eds.), (pp. 25–41). Oxford: British Ecological Society.

Hubbell, S., Foster, R., O'Brien, S., Harms, K., Condit, R., Wechsler, B., … de Lao, S. (1999). Light-gap disturbances, recruitment limitation, and tree diversity in a neotropical forest. Science, 283(5401), 554–557. 10.1126/science.283.5401.554

Hunter, M. O., Keller, M., Morton, D., Cook, B., Lefsky, M., Ducey, M., ... Schietti, J. (2015). Structural dynamics of tropical moist forest gaps. *PloS One*, *10*(7), e0132144. http://dx.doi.org/10.1371/journal.pone.0132144.

Hyyppä, J., Hyyppä, H., Leckie, D., Gougeon, F., Yu, X., & Maltamo, M. (2008). Review of methods of small-footprint airborne laser scanning for extracting forest inventory data in boreal forests. *International Journal of Remote Sensing*, *29*(5), 1339–1366. http://dx.doi.org/10.1080/01431160701736489.

Jaskierniak, D., Lane, P. N. J., Robinson, A., & Lucieer, A. (2011). Extracting LiDAR indices to characterise multilayered forest structure using mixture distribution functions. *Remote Sensing of Environment*, *115*(2), 573–585. http://dx.doi.org/10.1016/j.rse.2010.10.003.

Ke, Y., & Quackenbush, L. J. (2011). A review of methods for automatic individual tree-crown detection and delineation from passive remote sensing. *International Journal of Remote Sensing*, *32*(17), 4725–4747. http://dx.doi.org/10.1080/01431161.2010.494184.

Kent, R., Lindsell, J., Laurin, G., Valentini, R., & Coomes, D. (2015). Airborne LiDAR detects selectively logged tropical forest even in an advanced stage of recovery. *Remote Sensing*, *7*(7), 8348–8367. http://dx.doi.org/10.3390/rs70708348.

Lehmann, G. (2008). Label object representation and manipulation with ITK. *Insight Journal*, 1–34 Retrieved from http://en.scientificcommons.org/23203000

Lobo, E., & Dalling, J. W. (2014). Spatial scale and sampling resolution affect measures of gap disturbance in a lowland tropical forest: Implications for understanding forest regeneration and carbon storage. *Proceedings of the Royal Society of London B: Biological Sciences*, *281*. http://dx.doi.org/10.1098/rspb.2013.3218.

Malhi, Y., Doughty, C., & Galbraith, D. (2011). The allocation of ecosystem net primary productivity in tropical forests. *Philosophical Transactions of the Royal Society of London B: Biological Sciences*, *366*(1582), 3225–3245. http://dx.doi.org/10.1098/rstb.2011.0062.

Mallet, C., Lafarge, F., Roux, M., Soergel, U., Bretar, F., & Heipke, C. (2010). A marked point process for modeling lidar waveforms. *IEEE Transactions on Image Processing*. http://dx.doi.org/10.1109/TIP.2010.2052825.

Mascaro, J., Detto, M., Asner, G. P., & Muller-Landau, H. C. (2011). Evaluating uncertainty in mapping forest carbon with airborne LiDAR. *Remote Sensing of Environment*, *115*(12), 3770–3774. http://dx.doi.org/10.1016/j.rse.2011.07.019.

Medvigy, D., Wofsy, S. C., Munger, J. W., Hollinger, D. Y., & Moorcroft, P. R. (2009). Mechanistic scaling of ecosystem function and dynamics in space and time: Ecosystem demography model version 2. *Journal of Geophysical Research: Biogeosciences*, *114*(1), 1–21. http://dx.doi.org/10.1029/2008JG000812.

Meyer, V., Saatchi, S. S., Chave, J., Dalling, J. W., Bohlman, S., Fricker, G. a., ... Hubbell, S. (2013). Detecting tropical forest biomass dynamics from repeated airborne lidar measurements. *Biogeosciences*, *10*(8), 5421–5438. http://dx.doi.org/10.5194/bg-10-5421-2013.

Muller-Landau, H., Condit, R., Harms, K., Marks, C., Thomas, S., Bunyavejchewin, S., ... Ashton, P. (2006). Comparing tropical forest tree size distributions with the predictions of metabolic ecology and equilibrium models. *Ecology Letters*, *9*(5), 589–602. http://dx.doi.org/10.1111/j.1461-0248.2006.00915.x.

Ngomanda, A., Engone-Obiang, N., Lebamba, J., Moundounga-Mavouroulou, Q., Gomat, H., Mankou, G., ... Picard, N. (2014). Site-specific versus pantropical allometric equations: Which option to estimate the biomass of a moist central African forest? *Forest Ecology and Management*, *312*, 1–9. http://dx.doi.org/10.1016/j.foreco.2013.10.029.

Ploton, P., Barbier, N., Momo, S. T., Réjou-Méchain, M., Boyemba Bosela, F., Chuyong, G., ... Pélissier, R. (2015). Closing a gap in tropical forest biomass estimation: Accounting for crown mass variation in pantropical allometries. *Biogeosciences Discussions*, *12*(23), 19711–19750. http://dx.doi.org/10.5194/bgd-12-19711-2015.

Popescu, S. C., & Zhao, K. (2008). A voxel-based lidar method for estimating crown base height for deciduous and pine trees. *Remote Sensing of Environment*, *112*(3), 767–781. http://dx.doi.org/10.1016/j.rse.2007.06.011.

Saatchi, S., Mascaro, J., Xu, L., Keller, M., Yang, Y., Duffy, P., ... Schimel, D. (2015). Seeing the forest beyond the trees. *Global Ecology and Biogeography*, *24*(5), 606–610. http://dx.doi.org/10.1111/geb.12256.

Samet, H., & Tamminen, M. (1988). Efficient component labeling of images of arbitrary dimension represented by linear bintrees. *IEEE Transactions on Pattern Analysis and Machine Intelligence*, *10*(4), 579–586. http://dx.doi.org/10.1109/34.3918.

Shimizu, K., Ota, T., Kajisa, T., Mizoue, N., Yoshida, S., Takao, G., ... Vuthy, M. (2014). Estimation of aboveground biomass using manual stereo viewing of digital aerial photographs in tropical seasonal forest. *Land*, *3*(4), 1270–1283. http://dx.doi.org/10.3390/land3041270.

Silva, C., Crookston, N., Hudak, T., & Vierling, A. (2015). rLiDAR: LiDAR Data processing and visualization. r-cran. Retrieved from http://cran.at.r-project.org/web/packages/rLiDAR/index.html

Slik, J. W. F., Paoli, G., McGuire, K., Amaral, I., Barroso, J., Bastian, M., ... Zweifel, N. (2013). Large trees drive forest aboveground biomass variation in moist lowland forests across the tropics. *Global Ecology and Biogeography*, *22*(12), 1261–1271. http://dx.doi.org/10.1111/geb.12092.

Soininen, A. (2011). TerraScan User's guide. Available online at: http://www.terrasolid.fi/system/files/tscan_2.pdf(accessed: 6/07/2011).

Stark, S. C., Leitold, V., Wu, J. L., Hunter, M. O., de Castilho, C. V., Costa, F. R. C., ... Saleska, S. R. (2012). Amazon forest carbon dynamics predicted by profiles of canopy leaf area and light environment. *Ecology Letters*, *15*(12), 1406–1414. http://dx.doi.org/10.1111/j.1461-0248.2012.01864.x.

The CGAL Project (2015). *{CGAL} User and Reference Manual* (4.6 ed.). CGAL Editorial Board Retrieved from http://doc.cgal.org/4.6/Manual/packages.html

Tochon, G., Féret, J. B., Valero, S., Martin, R. E., Knapp, D. E., Salembier, P., ... Asner, G. P. (2015). On the use of binary partition trees for the tree crown segmentation of tropical rainforest hyperspectral images. *Remote Sensing of Environment*, *159*, 318–331. http://dx.doi.org/10.1016/j.rse.2014.12.020.

Ussyshkin, V., & Theriault, L. (2010). ALTM Orion: Bridging conventional lidar and full waveform digitizer technology. *The International Archives of the Photogrammetry, Remote Sensing and Spatial Information Sciences, XXXVIII*(*Part 7B*), 606–611.

White, E. P., Ernest, S. K. M., Kerkhoff, A. J., & Enquist, B. J. (2007). Relationships between body size and abundance in ecology. *Trends in Ecology and Evolution*, *22*(6), 323–330. http://dx.doi.org/10.1016/j.tree.2007.03.007.

Wulder, M. A., White, J. C., Nelson, R. F., Næsset, E., Ørka, H. O., Coops, N. C., ... Gobakken, T. (2012). Lidar sampling for large-area forest characterization: A review. *Remote Sensing of Environment*, *121*, 196–209. http://dx.doi.org/10.1016/j.rse.2012.02.001.

Zolkos, S. G., Goetz, S. J., & Dubayah, R. (2013). A meta-analysis of terrestrial aboveground biomass estimation using lidar remote sensing. *Remote Sensing of Environment*, *128*, 289–298. http://dx.doi.org/10.1016/j.rse.2012.10.017.